Amyloid-PET of the white matter: relationship to free water, fiber integrity, and cognition in patients with dementia and small vessel disease

Authors: Julie Ottoy[1*], Miracle Ozzoude[1*], Katherine Zukotynski[1,2,3,4], Min Su Kang[1,5], Sabrina Adamo[1], Christopher Scott[1], Joel Ramirez[1], Walter Swardfager[6], Benjamin Lam[7], Aparna Bhan[1], Parisa Mojiri[1], Alex Kiss[8], Stephen Strother[9,10], Christian Bocti[11], Michael Borrie[12], Howard Chertkow[13], Richard Frayne[14], Robin Hsiung[15], Robert Jr. Laforce[16], Michael D. Noseworthy[2,17], Frank S. Prato[12], Demetrios J. Sahlas[18], Eric E. Smith[19], Phillip H. Kuo[20], Jordan A. Chad[9,10], Ofer Pasternak[21], Vesna Sossi[15], Alexander Thiel[13], Jean-Paul Soucy[5], Jean-Claude Tardif[22], Sandra E. Black[1,7,†], Maged Goubran[1,9,23,†], for the Medical Imaging Trials Network of Canada (MITNEC) and Alzheimer's Disease Neuroimaging Initiative (ADNI) [**]

Affiliations:

[1]LC Campbell Cognitive Neurology Unit, Hurvitz Brain Sciences Program, Sunnybrook Research Institute, University of Toronto, Toronto, ON, Canada

[2]Departments of Medicine and Radiology, McMaster University, Hamilton, ON, Canada

[3]Department of Medical Imaging, Schulich School of Medicine & Dentistry, Western University, London, ON, Canada

[4]Department of Radiology, University of British Columbia, Vancouver, BC, Canada

[5]Montreal Neurological Institute, McGill University, Montreal, QC, Canada

[6]Department of Pharmacology & Toxicology, University of Toronto, Toronto, ON, Canada

[7]Department of Medicine (Division of Neurology), Dr. Sandra Black Centre for Brain Resilience and Recovery, Hurvitz Brain Sciences Research Program, Sunnybrook Health Sciences Centre, University of Toronto, Toronto, ON, Canada

[8]Department of Research Design and Biostatistics, Sunnybrook Research Institute, University of Toronto, Toronto, ON, Canada

[9]Department of Medical Biophysics, University of Toronto, Toronto, ON, Canada

[10]The Rotman Research Institute Baycrest, University of Toronto, Toronto, ON, Canada

[11]Service de Neurologie, Département de Medicine, Université de Sherbrooke, Sherbrooke, QC, Canada

[12]Lawson Health Research Institute, Western University, London, ON, Canada

[13]Jewish General Hospital and Department of Neurology and Neurosurgery, McGill University, Montreal, QC, Canada

[14]Departments of Radiology and Clinical Neuroscience, Hotchkiss Brain Institute, University of Calgary, Calgary, AB, Canada

[15]Physics and Astronomy Department and DM Center for Brain Health, University of British Columbia, Vancouver, BC, Canada

[16]Clinique Interdisciplinaire de Mémoire, Département des Sciences Neurologiques, Université Laval, Québec, QC, Canada

[17]Department of Electrical and Computer Engineering, McMaster University, Hamilton, ON, Canada

[18]Department of Medicine, McMaster University, Hamilton, ON, Canada

[19]Hotchkiss Brain Institute, University of Calgary, Calgary, AB, Canada

[20]Department of Medical Imaging, Medicine, and Biomedical Engineering, University of Arizona, Tucson, AZ, USA

[21]Departments of Psychiatry and Radiology, Brigham and Women's Hospital, Harvard Medical School, Boston, USA

[22]Montreal Heart Institute, Université de Montréal, Montreal, QC, Canada

[23]Physical Sciences Platform, Sunnybrook Research Institute, Sunnybrook Health Sciences Centre, Toronto, ON, Canada

** These authors contributed equally to this work*

† These authors contributed equally to this work

*** Data used in preparation of this article were obtained, in part, from the Alzheimer's Disease Neuroimaging Initiative (ADNI) database (adni.loni.usc.edu). As such, the investigators within the ADNI contributed to the design and implementation of ADNI and/or provided data but did not participate in analysis or writing of this report. A complete listing of ADNI investigators can be found at: http://adni.loni.usc.edu/wp-content/uploads/how_to_apply/ADNI_Acknowledgement_List.pdf*

Corresponding author:

Maged Goubran, Ph.D.

maged.goubran@utoronto.ca

+1-416-480-6100 Ext. 85410

2075 Bayview Avenue, M6 West RM 176

Toronto, Canada, M4N 3M5

Running headline: White matter amyloid-PET relates to free water

Abstract

White matter (WM) injury is frequently observed along with dementia. Positron emission tomography with amyloid-ligands (Aβ-PET) recently gained interest for detecting WM injury. Yet, little is understood about the origin of the altered Aβ-PET signal in WM regions. Here, we investigated the relative contributions of diffusion MRI-based microstructural alterations, including free water and tissue-specific properties, to Aβ-PET in WM and to cognition. We included a unique cohort of 115 participants covering the spectrum of low-to-severe white matter hyperintensity (WMH) burden and cognitively normal to dementia. We applied a bi-tensor diffusion-MRI model that differentiates between (i) the extracellular WM compartment (represented via free water), and (ii) the fiber-specific compartment (via free water-adjusted fractional anisotropy [FA]). We observed that, in regions of WMH, Aβ-PET related most closely to free water and WMH volume. In contrast, in normal-appearing WM, Aβ-PET related more closely to free water-adjusted FA and cortical Aβ. In relation to cognition, we observed a closer relationship with free water than with either free water-adjusted FA or WM PET. Our findings support free water and Aβ-PET as markers of WM abnormalities in patients with mixed dementia, and contribute to a better understanding of processes giving rise to the WM PET signal.

Keywords: Alzheimer's disease, amyloid-PET, diffusion MRI, free water, white matter

Introduction

^{18}F-Florbetapir (^{18}F-AV45) is one of the most commonly used PET ligands to detect and quantify amyloid-β (Aβ) burden in the cortex of patients with Alzheimer's disease (AD). Specifically, Aβ-ligands are thought to target the cross beta-sheet structure of the insoluble Aβ fibrils.[1] In addition to targeting fibrils in the cortex, these ligands are lipophilic in nature and show high retention in the white matter (WM).[1–3] It is hypothesized that their high WM uptake is due to a similar beta-sheet structure of myelin basic protein[4] and that microstructural damage or demyelination of WM tracts, previously observed in AD,[5] results in reduced ligand uptake.[6] Furthermore, while some reported the presence of Aβ deposits in the WM,[7,8] others did not observe such specific binding of the Aβ-ligand to WM tissue sections and attributed high WM retention to slow WM kinetics.[3,9,10] Further complexity of interpreting the WM PET signal is added through the existence of localized reduced blood-to-tissue transport, hypoperfusion of lesioned WM areas, and ligand trapping in enlarged perivascular spaces, particularly in patients with concomitant small vessel disease (SVD).[11] Taken together, the molecular basis of the Aβ-ligand binding to WM remains poorly understood, hindering the understanding and interpretation of Aβ-PET scans, especially in mixed disease cohorts.

Diffusion MRI (dMRI) is a useful imaging modality to study WM microstructure *in-vivo* and may help to better understand the binding dynamics of Aβ-ligands to WM.[12,13] Parameters derived from diffusion tensor imaging (DTI) modeling of dMRI data include fractional anisotropy (FA) and mean diffusivity (MD), commonly used to infer changes in fiber integrity.[14] Prior studies have shown lower FA and higher MD in areas of WM degradation such as those frequently observed as white matter hyperintensities (WMH) on Fluid Attenuated Inversion Recovery (FLAIR) MRI.[15] In addition, some found a link between lower FA and lower PET signal in the WM; thus supporting WM Aβ-PET as a marker of microstructural damage to myelin and/or axons.[12,16] However, this theory may be oversimplistic given that *single*-tensor DTI metrics (such as FA) are highly contaminated by signals from both adjacent cerebrospinal fluid (CSF) and freely diffusing water in the extracellular space surrounding the WM fiber tracts.[17,18] As such, conventional DTI metrics can hardly differentiate between degenerative and vascular/neuroinflammatory changes underlying altered Aβ-PET uptake in the WM. This bias will be exemplified in subjects with pronounced atrophy, enlarged CSF spaces, and vasogenic edema;[19,20] all of which are encountered in the more general AD population with often co-existent SVD pathology.[21]

Recently, a *bi*-tensor (two-compartment) model of dMRI was proposed to isolate the extracellular free water (FW) compartment from the fiber-specific (WM fibers) compartment within every image voxel.[22,23] In the human brain, FW is found as blood, interstitial fluid and CSF within ventricles and surrounding brain parenchyma, while it also accumulates as a form of edema in the extracellular spaces of structures distal from CSF such as deep WM.[22] Changes in FW may indicate extracellular processes including vascular damage and inflammation. On the other hand, changes in FW-adjusted DTI metrics (e.g., FW-adjusted FA) may be closer related to microstructural tissue damage, i.e. demyelination/axonal degeneration and fiber integrity.[22]

To our knowledge, no studies have yet investigated the link between Aβ-PET uptake in the WM and WM microstructure using multi-compartment diffusion modeling, specifically FW imaging. Particularly, such research is lacking in subjects with mixed Aβ and moderate-to-severe WM lesion burden. Therefore, our study aims to investigate the relative contributions of FW and tissue-specific microstructural changes to the ^{18}F-AV45 PET signal, both in regions of WMH and normal-appearing WM (NAWM), in a cohort enriched for high WMH burden. Our secondary aim is to investigate the microstructural properties and ^{18}F-AV45 PET of the WM in relation to cognition. We hypothesize that

lower PET signal within MRI-visible WM lesions closely relates to higher FW, which in turn, relates to cognitive impairment. Such research is imperative for more accurate interpretation of the Aβ-PET scan with potential as a future marker of WM abnormalities.

Material & Methods

Participants

The study included a total of 115 participants. Fifty-eight participants were recruited from dementia/stroke-prevention clinics as part of the multicenter C6 project of the Medical Imaging Network of Canada (MITNEC-C6) across seven participating sites. These participants showed moderate-to-severe SVD burden quantified as Fazekas-score>2 and confluent periventricular WMH volumes >10cc[24] [median(IQR): 31.1(22.4)cm^3]. Further inclusion criteria included: 1) clinical diagnosis of early AD or amnestic, non amnestic single or multi-domain mild cognitive impairment (MCI/AD, *N*=41),[25,26] or minor subcortical lacunar infarct/TIA (*N*=17); 2) age≥60y; 3) education>8y; and 4) MMSE≥20. Exclusion criteria included 1) major psychiatric disorder in the past 5y; 2) history of substance abuse in the past 2y; and 3) serious/chronic systemic or neurological illness (other than AD). Additionally, fifty-seven cognitively normal (CN) and patients with MCI were included from the Alzheimer's Disease Neuroimaging Initiative (ADNI-2) database with low-to-moderate WMH volumes [median(IQR): 5.8(9.2)cm^3]. Inclusion criteria included: 1) CN or MCI based on the absence (CN) or presence (MCI) of memory

complaints, MMSE≥24, and Clinical Dementia Rating of 0 (CN) or 0.5 (MCI); 2) age≥60y; and 3) education>8y. More details on inclusion/exclusion criteria in MITNEC-C6 and ADNI are described in **Supplementary Table 1** and at www.adni-info.org. **Table 1** describes demographics for both groups (i.e., ADNI-2 and MITNEC-C6, further referred to as the *low* and *high* WMH group, respectively). Both groups were matched for vascular risk factors including hypertension, pulse pressure, body mass index, sex, and smoking status.[27] All participants underwent ^{18}F-AV45 PET, 3T MRI including 3D T1, FLAIR, and dMRI, and a neuropsychological assessment. MRI–PET and MRI–neuropsychology acquisitions were acquired in close proximity (54±80 and 27±78 days ± standard deviation, respectively).

Standard Protocol Approvals, Registrations, and Patient Consents

All imaging acquisition protocols were standardized across vendor platforms and compatible with ADNI-2 (see acquisition parameters in **Supplementary Table 2)**.[28] Image quality control, archiving of clinical and imaging data, and access to pipelines were performed at the Sunnybrook Research Institute through a common database. All participants provided written informed consent. This study was conducted in full

conformance with the principles of the “Declaration of Helsinki”. The institutional review board at the Sunnybrook Research Institute approved this study (Approval No. MI1-112246).

Regarding ADNI data; ADNI was launched in 2003 as a public-private partnership. The primary goal of ADNI was to test whether MRI, PET, other biological markers, and clinical data can be combined to measure the progression of MCI/AD [see www.adni-info.org].

Cognitive Screening Tests

Cognitive screening tests used for this study are previously described[27] and included processing speed and executive function (attention switching and working memory) measured with the Trail Making Test (TMT) parts A (TMT-A; *N*=115) and B (TMT-B; *N*=114), semantic fluency with animal naming (*N*=115), language with Boston Naming Test (BNT; *N*=109), and global cognition with the Montreal Cognitive Assessment (MoCA) and the Mini-Mental State Examination (MMSE) (*N*=115). TMT test scores were log-transformed to achieve a normal distribution.

Structural MRI

MRI was performed using acquisition protocols that were standardized across vendor platforms and compatible with the ADNI-2 protocol (see acquisition parameters in **Supplementary Table 2)**.[28] The T1-weighted (T1w) MRI images were processed with FreeSurfer v6.0 using an in-house modified pipeline for subjects with SVD.[29] Subcortical lacunar infarcts were masked out before WMH segmentation.[30] WMH were delineated based on our automated segmentation tool HyperMapper.[31] More details on MRI processing are described in **Supplementary methods S1**. Total WMH volume was normalized by the total intracranial volume (ICV), and log-transformed. Total ICV was estimated using a skull-stripping deep learning network developed in-house that is robust to vascular lesions and atrophy.[32]

The NAWM was segmented in native space by subtracting the binarized WMH regions from the binarized whole WM defined by the Desikan-Killiany-Tourville atlas. To limit partial volume effects, we 1) did not include ADNI subjects with WMH <1,000mm^3 (no MITNEC-C6 subjects fulfilled this criterion), 2) used a stricter HyperMapper threshold

on segmentation probabilities (0.4-0.5) to avoid overestimation of WMH,[31] and 3) performed erosion on the NAWM masks by 2x2x2mm^3 to eliminate spill-effects from neighboring tissue including cortex and CSF. **Figure 1**A highlights WMH and NAWM delineations in an example subject.

Diffusion tensor imaging

Raw ADNI data was downloaded from the ADNI-2 database. Acquisition parameters included 256×256 matrix size, 1.4×1.4×2.7mm^3 voxel size, 9000ms TR, and 9min scan time. A total of 41 diffusion encoding directions (b=1000s/mm^2) and five b=0s/mm^2 were acquired. More details can be found at http://adni.loni.usc.edu/wp-content/uploads/2010/05/ADNI2_GE_3T_22.0_T2.pdf. In MITNEC-C6, dMRI scans were acquired using a 128×128 matrix size, 2mm isotropic voxels, TR ranging between 9400 and 10000ms and 30 or 32 directions depending on the vendor with b=1000s/mm^2 and two b=0s/mm^2. Full acquisition protocols are included in **Supplementary Table 2.** The preprocessing steps to obtain corrected dMRI data and DTI scalar maps (FA and MD) are in line with Nir et al.[33] and described in more detail in **Supplementary methods S2**.

For FW mapping, the eddy current and motion-corrected dMRI data were fitted to a two-compartment diffusion model in each voxel, separating the FW compartment from the non-FW tissue compartment (**Figure 1**B).[22] Specifically, an FW map represents the fractional volume (ranging from 0 to 1) of freely diffusing extracellular water with a fixed isotropic diffusivity of 3×10^{-3} mm^2/s (diffusion coefficient of water at body temperature). The FW-corrected FA represents the FA signal following removal of the FW signal and is expected to be more specific to axonal and myelination changes than FA alone (**Figure 1**B).[17] Subsequently, the mean FA, MD, FW, and FW-adjusted FA were extracted in the whole brain, WMH, and NAWM. **Figure 1**A shows an example of a T1w image with corresponding DTI-based scalar maps.

FW correlated strongly (Pearson's $r > 0.5$) with both FA and MD in WMH and with FA in NAWM, but not with FW-adjusted FA indicating that the FW effect was indeed removed from FW-adjusted FA (**Supplementary Figure 1**).

Amyloid-PET imaging

Details on acquisition and processing of ^{18}F-AV45 scans are described in **Supplementary methods S3**. Standardized uptake value ratios (SUVR) were generated in the WMH and NAWM masks within the native T1w space and referenced to the whole cerebellum. A 'global' Aβ SUVR value was derived based on the AD-signature regions (volume-weighted average of the frontal, parietal, temporal, and cingulate regions)[34] and corrected for partial volume effects.

Statistical analyses

Statistics were performed using Python v3.7, R v4.0, and PROCESS v3.5 in SPSS. All continuous metrics were z-scored. Model-based measures were reported as effect estimates and 95% confidence intervals (CI) based on bootstrapping with 1,000 replications. A paired t-test was used to detect significant differences in SUVR or DTI metrics between NAWM and WMH.

1. Relationship between ^{18}F-AV45 SUVR and DTI metrics

Linear regressions were used to assess the associations between each of the DTI metrics (independent variable) and SUVR (dependent variable) in NAWM or WMH, adjusted for continuous age and education, and sex. The regressions evaluated in the WMH were additionally adjusted for global cortical Aβ SUVR and for WMH volume. The regressions evaluated in the NAWM were adjusted for global cortical Aβ SUVR; WMH volume was not significantly associated with NAWM SUVR and thus omitted as covariate ($P>0.05$). All regressions were evaluated across all subjects as well as within the high WMH group separately. We did not investigate regressions within the low WMH group separately due to the limited resolution associated with PET signals in small WMH volumes.

Partial least square (PLS) regression analyses were performed to further investigate how the closely related DTI metrics, as well as demographical (age, sex, education) and imaging (WMH volume, cortical Aβ SUVR) variables, covary together in predicting SUVR in the WMH or NAWM. The number of components was determined based on the root-mean-square error derived from a ten-fold cross-validation with five repeats.

2. Relationship with cognitive impairment

Linear regression analysis was employed to assess the associations between DTI metrics in WMH or NAWM (FW and FW-adjusted FA; independent variable) and cognitive scores (dependent variable), adjusted for age, sex, education, WMH volume, and global cortical Aβ SUVR. In addition, the relationship between SUVR in the WMH or NAWM and cognition was investigated with mediation analysis using FW or FW-adjusted FA as the mediators, adjusted for age, sex, and education. Bias-corrected bootstrapping with 5,000 replications and a 95% CI was performed for estimation of (in)direct and total effects.

3. Linear mixed-effect models

To investigate the effects of age or sex on ^{18}F-AV45 SUVR in the WM, we employed linear mixed effect models with an interaction term between age or sex and WM region (NAWM and WMH) and subject as a random factor.

Data and materials availability

All data associated with this study are available in the main text or supplementary materials. All the imaging data can be shared upon request with a proposal and under a data transfer agreement.

Results

Demographics

The high WMH group (*N*=58) was significantly older and less educated compared to the low WMH group (*N*=57). Additionally, they had significantly higher cortical Aβ load and lower cognitive scores (**Table 1**). The proportion of Aβ-positive subjects was 22.8% and 46.6% in the low and high WMH group, respectively.

^{18}F-AV45 SUVR and DTI metrics are altered in WMH compared to NAWM

Regions of WMH showed significantly lower SUVR compared to NAWM (~14% reduction, t=25.08, P<0.0001) (**Figure 2**). In addition, regions of WMH showed

significantly higher FW (t=-27.11), higher MD (t=-24.37), lower FA (t=32.77), and lower FW-adjusted FA (t=12.26) compared to NAWM (all P<0.0001; **Figure 2**).

^{18}F-AV45 SUVR relates to FW in WMH and to FW-adjusted FA in NAWM

In regions of WMH, lower SUVR was strongly associated with higher FW both across all subjects (β=-0.36, P=0.005; 95%$CI_{bootstrap}$[-0.63,-0.10]) (**Figure 3**A-left) and in the high WMH group separately (β=-0.33, P=0.019; 95%$CI_{bootstrap}$[-0.55,-0.06]); results were not investigated in the low WMH group due to the limited resolution associated with PET signal in small WMH volumes. In addition, in regions of WMH, lower SUVR was associated with lower FA (β=+0.24, P=0.046; 95%$CI_{bootstrap}$[+0.008,+0.47]) and showed a trend with higher MD (P=0.064; 95%$CI_{bootstrap}$[-0.44,+0.003]) across all subjects, but not with the fiber-specific metric FW-adjusted FA. Taken together, these results indicate that, amongst the DTI metrics, FW was most closely associated with ^{18}F-AV45 SUVR in regions of WMH.

In the NAWM, SUVR was inversely associated with FW-adjusted FA in the high WMH group (β=-0.32, P=0.008; 95%$CI_{bootstrap}$[-0.53,-0.07]) and showed a trend across all

subjects (P=0.077; 95%$CI_{bootstrap}$[-0.32,+0.05]). In addition, there was a trend towards an association between lower SUVR and higher FW across all subjects (P=0.059; 95%$CI_{bootstrap}$[-0.38,+0.05]; **Figure 3**A-right), while no associations were found with MD or FA in the NAWM. Taken together, these results indicate that, amongst the DTI metrics, FW-adjusted FA was most closely associated with ^{18}F-AV45 SUVR in the NAWM.

Our findings were further confirmed by PLS analysis of WM SUVR with DTI metrics. In regions of WMH, FW and WMH volume loaded most strongly inversely onto the first component (24% variance), while FW-adjusted FA and FA also had a significant but smaller contribution (**Figure 3**B-left; high WMH group). This may indicate that lower SUVR in regions of WMH is associated with both higher FW and WMH volume but to a lesser extent with FW-adjusted FA. On the other hand, in NAWM, cortical Aβ SUVR loaded most strongly positively onto the first component (31% variance), while FW-adjusted FA loaded significantly in an inverse way (**Figure 3**B-right; high WMH group). This may indicate that higher SUVR in NAWM is associated with higher cortical Aβ together with lower FW-adjusted FA. Similar results with PLS analysis were found with all subjects combined, i.e. FW, WMH volume, and FA consistently contributed to ^{18}F-AV45

SUVR in WMH, while FW-adjusted FA did not contribute to the first components (**Supplementary Figure 2**).

Increased FW in WM is associated with cognitive impairment

In regions of WMH, higher FW was associated with worse performance on the MoCA, MMSE, language, and semantic fluency tests both across all subjects and in the high WMH group separately (**Figure 4**A; **Table 2**). In fact, higher FW mediated the relationship between SUVR and executive function ($\beta_{indirect}$=-0.06, 95%$CI_{bootstrap}$[-0.14,-0.01]). Conversely, lower FW-adjusted FA was significantly associated only with lower MoCA scores across all subjects.

Similarly, in the NAWM, higher FW was associated with worse performance on the MoCA, MMSE, language, and semantic fluency tests both across all subjects and in the high WMH group separately (**Figure 4**B; **Table 2**). Conversely, lower FW-adjusted FA in the NAWM was significantly associated only with lower MMSE across all subjects.

Effects of age and sex on ^{18}F-AV45 SUVR in the WM

We observed a significant interaction effect (P<0.0001) between age and WM regions (i.e., NAWM vs WMH) on SUVR, such that older age was associated with lower SUVR in the WMH but with higher SUVR in the NAWM (**Supplementary Figure 3**). Females showed consistently higher SUVR in both NAWM (P=0.008) and WMH (P=0.006) compared to males, with no observed interaction (**Supplementary Figure 4**).

Discussion

This study investigated the neurobiological underpinnings of Aβ-PET (^{18}F-AV45) uptake in the WM using two-compartment modelling of diffusion MRI in a mixed cohort of patients with mild-to-severe SVD (manifested as WMH) and cortical Aβ. In line with current literature, we observed that SUVR in regions of WMH was significantly decreased compared to the NAWM SUVR.[12,13,16] Our manuscript led to three novel observations (summary **Figure 5**): 1) In WMH, the decrease in SUVR was closely related to higher FW; 2) In NAWM, the increase in SUVR was closely related to higher cortical Aβ and lower FW-adjusted FA; and 3) In both WMH and NAWM, higher FW was related to cognitive impairment and mediated the association between WMH SUVR and executive function.

These findings can be interpreted as following: 1) The lower PET signal in WMH may largely reflect vascular damage, edema, inflammation, and/or fiber necrosis that lead to concomitant enlargement of the extracellular space; 2) The higher PET signal in NAWM tracks with cortical Aβ and may partly reflect microstructural damage to the remaining fibers; and 3) FW may be a sensitive SVD-related biomarker in AD and mixed dementia to detect early and more subtle changes in WM microstructure.

Supported by previous evidence that myelin alterations represent an early feature of aging and AD,[5] Aβ-PET in the WM was recently suggested as a marker of local myelin integrity;[12,13,16] thereby adding value to quantifying Aβ in the cortex. However, prior studies did not account for contributions of FW to the conventional DTI metrics (such as FA), ultimately limiting their interpretation and potentially overestimating the level of demyelination or axonal damage.[18,35] While we confirm prior studies by reporting an association between lower Aβ SUVR and lower FA (before FW adjustment) in WMH regions,[12] we notably showed that the lower SUVR was more strongly associated with FW than with either FA or FW-adjusted FA. This lower SUVR in WMH was also associated with higher WMH volume. These findings may indicate that the PET signal within MRI-visible WM lesions is more profoundly associated with enlargement of the extracellular

space (potentially of vascular or inflammatory origin, reflecting profound tissue loss/necrosis)[22,36] than with tissue-specific compartment alterations (e.g., reduced fiber integrity or localized demyelination).[37] Several additional considerations may support this observation. First, while demyelinating fibers are an early feature in AD,[5] their effects on the diffusion metrics may be less pronounced in a sample enriched for SVD.[35] Indeed, our group has previously shown that WM disease may primarily reflect chronic vasogenic edema (blood-brain barrier [BBB] leakage) or perivascular stasis (compromised circulation of interstitial fluid) induced by venous collagenosis;[19,20] together with some degree of neuroinflammation, damage to myelin membranes with potential formation of intramyelinic fluid-filled vacuoles, and axonal degeneration in cases with concomitant AD pathology.[35,36] Second, previous autopsy studies reported a lack of PiB binding to WM tracts,[3,9] suggesting that demyelination alone does not account for the reduced PET signal. Taken together, we speculate that reduced ^{18}F-AV45 retention in MRI-visible WM lesions is at least partly reflective of increased water content.

In NAWM, the relation of SUVR with FW-adjusted FA was stronger than with either FA or FW (**Figure 5**). This may be related to a lesser expansion of the extracellular space in NAWM. Interestingly, while lower FW-adjusted FA is typically interpreted as

reduced fiber integrity, we observed a relationship between lower SUVR and higher (rather than lower) FW-adjusted FA in the whole NAWM. There are several potential explanations for this finding. First, higher FW-adjusted FA may represent the loss of crossing fibers, consistent with degeneration of selected tracts, as previously observed in patients with MCI or AD.[38,39] Second, we observed, similar to prior work, that cortical and NAWM SUVRs are positively correlated even after partial volume correction/erosion.[12,40–42] This may indicate that cortical AD pathology is one of the drivers behind (i) increased NAWM PET, and (ii) decreased FW-adjusted FA (either through direct WM injury or secondary Wallerian degeneration).[5,43] One potential explanation for this positive cortex-NAWM SUVR relationship, considering that NAWM was heavily eroded, may be impaired CSF-mediated clearance and presence of Aβ deposits in vessel walls, commonly observed in AD. Specifically, vascular Aβ may block drainage pathways (along the basement membranes in walls of capillaries and arteries) causing retrograde enlargement of perivascular spaces and WM lesions, in turn, reinforcing impaired clearance of toxic Aβ solutes.[44,45] Prior work suggested that periventricular WMH partly represent vasogenic edema related to leakage from venules stenosed or occluded with collagen.[19] Thus, the resulting periventricular venous insufficiency may interfere with interstitial cerebral fluid circulation, impairing the drainage of Aβ along the periarteriolar vascular spaces and

promoting Aβ deposition as plaques and around the vessels.[46] Another potential explanation for this relationship may be related to our finding that both metrics increase with age, in line with others (**Figure 5**).[12]

These observations have several implications in clinical and research settings. First, the close relationship between the FW and PET signals in this cohort challenges previous reports suggesting that the WM PET signal is myelin-dominated based on conventional FA. Our observations thus contribute to a better understanding and more accurate interpretation of the ambiguous WM signal in ^{18}F-AV45 PET; this is of particular importance as Aβ-PET imaging is increasingly used in routine clinical practice for diagnostic workup of patients with suspect AD or mixed dementia, as well as for patient enrichment and target evaluation of anti-Aβ treatment trials. Second, in elderly subjects with suspicious areas of (low-to-moderate) cortical Aβ, who also have high WMH burden and atrophy, the cortical Aβ-PET signal may visually appear artificially reduced by the spill-in from low WMH-associated signals, potentially leading to a false negative reading. On the other hand, in patients with substantial cortical Aβ and WMH, the cortex-WM contrast may visually appear enhanced (despite spill-over effects at the cortex-WM boundary). Third, although lower FW-adjusted FA did not translate into a lower SUVR signal in the *whole* NAWM, we found a reduction

of SUVR in the NAWM in subjects with >30cc WMH volumes (**Supplementary Figure 5**). This may be due to microstructural changes spreading beyond the visible damage of the WMH (assessed on structural imaging) into the surrounding penumbras (peri-lesional areas) of WMH and connected tracts.[43,47] Thus, the spectrum of WM damage identified by PET may be wider than that identified by T1w or FLAIR sequences where more subtle microstructural changes may not manifest as contrast changes and can be hard to identify. Another important implication of the altered PET signal in WM, particularly to research applications, is that it will affect the use of WM as a reference region to quantify cortical Aβ SUVR. Future studies should mask out WMH from the WM reference region, erode their WM masks, and/or use WMH volume as a covariate in the analyses. They should also compare WM SUV between diagnostic groups to assure no significant differences in reference region uptake.[2,48]

In relation to cognition, we observed that higher FW was associated with cognitive impairment both in regions of WMH and NAWM. The association in the NAWM may potentially reflect mild vascular damage and an early, pre-lesional role for FW in affecting cognitive function.[23] Apart from the significant FW-cognition relationship, we observed that FW (but not FW-adjusted FA) mediated the association between PET and executive

function in WMH. In fact, FW-adjusted FA only showed a weak relationship with MoCA within WMH and with MMSE within NAWM (the sensitivity of MoCA to WMH may be related to its wider application as a screening tool for vascular cognitive impairment by covering domains of executive function)[49]. Similarly, Maillard et al.[50] found that FW fully mediated the effect of WMH volume on cognition among older adults, while they reported a lack of association between FW-adjusted FA and cognition. Taken together, these findings underscore FW as a potential biomarker in early dementia stages, following its appearance and clinical relevance in both pre-lesional and MRI-visible lesions of the WM. Thus, eliminating or preventing excessive FW in the WM may serve as a potential preventive strategy (e.g., through earlier, more personalized vascular risk control) against vascular injury, cognitive decline, and progression to AD dementia.

Limitations of our study include the use of single-shell dMRI and static PET imaging. Thus, we cannot investigate whether WM PET may be affected by altered BBB permeability and/or the ligand's pharmacokinetics through slower perfusion in WMH.[11,51] Prior work with ^{18}F-AV45 has shown that a 20% reduction in WM blood perfusion was associated with less than 5% reduction in SUVR at 50-60min post-injection;[52] as such, we do not believe that that the ~14% reduction in WMH SUVR (compared to NAWM) would

be fully attributable to changes in blood perfusion. Second, we focused on the averaged PET and DTI metrics within the NAWM and WMH. Thus, we cannot exclude that the FW-adjusted tissue compartment had more regional or tract-specific associations with Aβ-PET and cognitive performance.[23]

A major strength of our work is the inclusion of real-world patients covering the spectrum of low to severe WMH burden and cortical Aβ deposition. Specifically, seventy-eight subjects (~70%) had WMH>10cc, allowing us to more accurately account for partial volume effects which are prominent in most dementia studies with small WMH burden such as ADNI. In addition, by leveraging a novel dMRI technique that adjusts FA for FW contributions, as well as optimized structural pipelines for high WMH burden including a state-of-the-art deep learning segmentation model, we provided novel insights into the relationship of WM microstructure with the ^{18}F-AV45 signal in the WM.

In conclusion, this study investigated the neurobiological underpinnings of Aβ-PET (^{18}F-AV45) uptake in the WM – a marker of WM injury that is extracted "for free" in the diagnostic workup of dementia – using advanced diffusion modelling in a WMH enriched cohort. We found that lower ^{18}F-AV45 PET uptake in MRI-visible WM lesions is strongly

linked to elevated FW, potentially reflecting vascular damage, edema, inflammation, and/or proportional loss of WM tissue. On the other hand, in the NAWM, the ^{18}F-AV45 PET uptake was more closely associated with Aβ of the cortex and alterations to WM fiber integrity. We also highlighted that WM PET may be sensitive to microstructural changes in the penumbras surrounding WMH that are not yet visible on structural imaging. Last, in relation to cognition, higher FW both in WM lesions and NAWM related more closely to cognitive impairment than FW-adjusted FA or WM PET. Our study contributed to important new insights into the biological processes underlying the altered PET signal in the WM, further aiding in the interpretation of Aβ-PET studies. In addition, we present evidence that supports the need for accounting for WM lesions in Aβ-PET analyses and considerations for using WM as a reference region. Finally, we highlighted FW as a promising and potentially early vascular-related injury marker in AD.

Acknowledgements: We would like to express our deepest gratitude towards all the participants and caregivers for their support and participation in this study. We are grateful for the support of the Medical Imaging Trial Network of Canada (MITNEC; https://clinicaltrials.gov/ct2/show/NCT02330510?term=mitnec+sandra+black&rank=1) Grant #NCT02330510, and to Eli Lilly & Company for providing the 18F-florbetapir ligand. In addition, part of the data collection and sharing for this project was funded by ADNI (National Institutes of Health Grant U01 AG024904) and DOD ADNI (Department of Defense award number W81XWH-12-2-0012). ADNI is funded by the National Institute on Aging, the National Institute of Biomedical Imaging and Bioengineering, and through generous contributions from the following: AbbVie, Alzheimer's Association; Alzheimer's Drug Discovery Foundation; Araclon Biotech; BioClinica, Inc.; Biogen; Bristol-Myers Squibb Company; CereSpir, Inc.; Cogstate; Eisai Inc.; Elan Pharmaceuticals, Inc.; Eli Lilly and Company; EuroImmun; F. Hoffmann-La Roche Ltd and its affiliated company Genentech, Inc.; Fujirebio; GE Healthcare; IXICO Ltd.; Janssen Alzheimer Immunotherapy Research & Development, LLC.; Johnson & Johnson Pharmaceutical Research & Development LLC.; Lumosity; Lundbeck; Merck & Co., Inc.; Meso Scale Diagnostics, LLC.; NeuroRx Research; Neurotrack Technologies; Novartis Pharmaceuticals Corporation; Pfizer Inc.; Piramal Imaging; Servier; Takeda Pharmaceutical Company; and

Transition Therapeutics. The Canadian Institutes of Health Research provided some funding to support ADNI clinical sites in Canada. Private sector contributions are facilitated by the Foundation for the National Institutes of Health (www.fnih.org). The grantee organization is the Northern California Institute for Research and Education, and the study is coordinated by the Alzheimer's Therapeutic Research Institute at the University of Southern California. ADNI data are disseminated by the Laboratory for Neuro Imaging at the University of Southern California.

Funding: This study was funded by the Canadian Institute for Health Research (CIHR) MOP Grant #13129, CIHR Foundation grant #159910, the L.C Campbell Foundation and the SEB Centre for Brain Resilience and Recovery. The work was also supported by the Medical Imaging Trial Network of Canada (MITNEC) Grant #NCT02330510. JO is supported by the Alzheimer's Association fellowship (AARF-21-848556). MG is supported by Gerald Heffernan foundation, the Donald Stuss Young Investigator innovation award, and CIHR Grant #PJT178059.

Authors' contributions: JO, MO, MG, and SEB designed the study and experiments. JO and MO wrote the manuscript, analyzed and interpreted the data with input from MG and SEB.

MSK, KZ, PHK, WS, SA, CS, JR, AP, PM, and BL contributed to data generation, interpretation, and revision. JAC and OP contributed to toolbox development and revised the manuscript. AK, SS, CB, MB, HC, RF, RH, RJL, MDN, FSP, DJS, EES, VS, AT, JPS, and JCT participated in the study concept and design as site leaders and revised the manuscript. MG and SEB supervised all aspects of this work.

Declaration of conflicting interests: Dr. Black has received in kind support for PET ligands from GE Healthcare and Eli Lilly Avid. She has received personal fees for educational talks from Biogen and for advisory committees from Biogen and Hoffmann La Roche. She is a Principal Investigator or Sub Investigator for clinical trials with funding to the institution only for the following companies: Hoffmann La Roche, Biogen Eisai, Eli Lilly, UCB Biopharma SRL, Novo Nordisk, and Alector Inc.; Dr. Tardif reports research grants from Amarin, AstraZeneca, Ceapro, DalCor Pharmaceuticals, Esperion, Ionis, Novartis, Pfizer, RegenXBio and Sanofi; honoraria from AstraZeneca, DalCor Pharmaceuticals, HLS Pharmaceuticals and Pendopharm; minor equity interest from DalCor Pharmaceuticals; and authorship of patents on pharmacogenomics-guided CETP inhibition, use of colchicine after myocardial infarction, and use of colchicine for coronavirus infection (Dr. Tardif waived his rights in the colchicine patents); Dr. Bocti reports an investment in IMEKA; Dr.

Noseworthy is the CEO/director and cofounder of TBIfinder Inc.; Dr. Kuo is an employee of Invicro. He is a consultant and/or speaker for Amgen, Bayer, Chimerix, Eisai, Fusion Pharma, General Electric Healthcare, Invicro, Novartis, and UroToday. He is a recipient of research grants from Blue Earth Diagnostics and General Electric Healthcare; Dr. Strother is a shareholder and senior scientific consultant for ADMdx, Inc., which receives NIH funding, and this work was partly supported by research grants from Canadian Institutes of Health Research (CIHR), and the Ontario Brain Institute in Canada; Dr. Smith consulted for Eli Lilly and for the Data Safety Monitoring Board for the U.S. NIH; Dr. Borrie is the Medical Director for the Aging Brain and Memory Clinic, an investigator with the Cognitive Clinical Research Group (CCRG), Past President of the Consortium for Canadian Centres for Clinical Cognitive Research (C5R). He is the platform lead for the Comprehensive Assessment of Neurodegeneration and Aging (COMPASS-ND) observational study of the Canadian Collaboration on Neurodegeneration in Aging (CCNA). Since 1995 the CCRG has been a leading Canadian research site conducting randomized controlled trials of new potential treatments for Subjective Cognitive Decline, Mild Cognitive Impairment and Alzheimer's Disease.

References

1 Choi SR, Golding G, Zhuang Z, Zhang W, Lim N, Hefti F *et al.* Preclinical Properties of ^{18}F-AV-45: A PET Agent for Aβ Plaques in the Brain. *J Nucl Med* 2009; **50**: 1887–1894.

2 Ottoy J, Verhaeghe J, Niemantsverdriet E, Wyffels L, Somers C, De Roeck E *et al.* Validation of the Semiquantitative Static SUVR Method for ^{18}F-AV45 PET by Pharmacokinetic Modeling with an Arterial Input Function. *J Nucl Med* 2017; **58**: 1483–1489.

3 Fodero-Tavoletti MT, Rowe CC, McLean CA, Leone L, Li Q-X, Masters CL *et al.* Characterization of PiB binding to white matter in Alzheimer disease and other dementias. *J Nucl Med* 2009; **50**: 198–204.

4 Harauz G, Ishiyama N, Hill CMD, Bates IR, Libich DS, Farès C. Myelin basic protein—diverse conformational states of an intrinsically unstructured protein and its roles in myelin assembly and multiple sclerosis. *Micron* 2004; **35**: 503–542.

5 Dean DC III, Hurley SA, Kecskemeti SR, O'Grady JP, Canda C, Davenport-Sis NJ *et al.* Association of Amyloid Pathology With Myelin Alteration in Preclinical Alzheimer Disease. *JAMA Neurology* 2017; **74**: 41–49.

6 Stankoff B, Freeman L, Aigrot M-S, Chardain A, Dollé F, Williams A *et al.* Imaging central nervous system myelin by positron emission tomography in multiple sclerosis using [methyl-11C]-2-(4′-methylaminophenyl)- 6-hydroxybenzothiazole. *Ann Neurol* 2011; **69**: 673–680.

7 Iwamoto N, Nishiyama E, Ohwada J, Arai H. Distribution of amyloid deposits in the cerebral white matter of the Alzheimer's disease brain: relationship to blood vessels. *Acta Neuropathologica* 1997; **93**: 334–340.

8 Collins-Praino LE, Francis YI, Griffith EY, Wiegman AF, Urbach J, Lawton A *et al.* Soluble amyloid beta levels are elevated in the white matter of Alzheimer's patients,

independent of cortical plaque severity. *Acta Neuropathologica Communications* 2014; **2**: 83.

9 Hong YT, Veenith T, Dewar D, Outtrim JG, Mani V, Williams C *et al.* Amyloid Imaging With Carbon 11–Labeled Pittsburgh Compound B for Traumatic Brain Injury. *JAMA Neurol* 2014; **71**: 23.

10 Heurling K, Buckley C, Vandenberghe R, Laere KV, Lubberink M. Separation of β-amyloid binding and white matter uptake of 18F-flutemetamol using spectral analysis. *Am J Nucl Med Mol Imaging* 2015; **5**: 515–526.

11 Wright P, Veronese M, Mazibuko N, Turkheimer FE, Rabiner EA, Ballard CG *et al.* Patterns of Mitochondrial TSPO Binding in Cerebral Small Vessel Disease: An in vivo PET Study With Neuropathological Comparison. *Frontiers in Neurology* 2020; **11**.

12 Zeydan B, Schwarz CG, Lowe VJ, Reid RI, Przybelski SA, Lesnick TG *et al.* Investigation of white matter PiB uptake as a marker of white matter integrity. *Ann Clin Transl Neurol* 2019; **6**: 678–688.

13 Goodheart AE, Tamburo E, Minhas D, Aizenstein HJ, McDade E, Snitz BE *et al.* Reduced binding of Pittsburgh Compound-B in areas of white matter hyperintensities. *Neuroimage Clin* 2015; **9**: 479–483.

14 Concha L. A macroscopic view of microstructure: Using diffusion-weighted images to infer damage, repair, and plasticity of white matter. *Neuroscience* 2014; **276**: 14–28.

15 Maniega SM, Valdés Hernández MC, Clayden JD, Royle NA, Murray C, Morris Z *et al.* White matter hyperintensities and normal-appearing white matter integrity in the aging brain. *Neurobiol Aging* 2015; **36**: 909–918.

16 Moscoso A, Silva-Rodríguez J, Aldrey JM, Cortés J, Pías-Peleteiro JM, Ruibal Á *et al.* 18F-Florbetapir PET as a marker of myelin integrity across the Alzheimer's disease spectrum. *Eur J Nucl Med Mol Imaging* 2021. doi:10.1007/s00259-021-05493-y.

17 Metzler-Baddeley C, O'Sullivan MJ, Bells S, Pasternak O, Jones DK. How and how not to correct for CSF-contamination in diffusion MRI. *NeuroImage* 2012; **59**: 1394–1403.

18 Berlot R, Metzler-Baddeley C, Jones DK, O'Sullivan MJ. CSF contamination contributes to apparent microstructural alterations in mild cognitive impairment. *NeuroImage* 2014; **92**: 27–35.

19 Keith J, Gao F-Q, Noor R, Kiss A, Balasubramaniam G, Au K *et al.* Collagenosis of the Deep Medullary Veins: An Underrecognized Pathologic Correlate of White Matter Hyperintensities and Periventricular Infarction? *J Neuropathol Exp Neurol* 2017; **76**: 299–312.

20 Pettersen JA, Keith J, Gao F, Spence JD, Black SE. CADASIL accelerated by acute hypotension: Arterial and venous contribution to leukoaraiosis. *Neurology* 2017; **88**: 1077–1080.

21 Toledo JB, Arnold SE, Raible K, Brettschneider J, Xie SX, Grossman M *et al.* Contribution of cerebrovascular disease in autopsy confirmed neurodegenerative disease cases in the National Alzheimer's Coordinating Centre. *Brain* 2013; **136**: 2697–2706.

22 Pasternak O, Sochen N, Gur Y, Intrator N, Assaf Y. Free water elimination and mapping from diffusion MRI. *Magnetic Resonance in Medicine* 2009; **62**: 717–730.

23 Ji F, Pasternak O, Liu S, Loke YM, Choo BL, Hilal S *et al.* Distinct white matter microstructural abnormalities and extracellular water increases relate to cognitive impairment in Alzheimer's disease with and without cerebrovascular disease. *Alz Res Therapy* 2017; **9**: 63.

24 DeCarli C, Murphy DGM, Tranh M, Grady CL, Haxby JV, Gillette JA *et al.* The effect of white matter hyperintensity volume on brain structure, cognitive performance, and cerebral metabolism of glucose in 51 healthy adults. *Neurology* 1995; **45**: 2077–2084.

25 McKhann GM, Knopman DS, Chertkow H, Hyman BT, Jack CR, Kawas CH *et al.* The diagnosis of dementia due to Alzheimer's disease: Recommendations from the National Institute on Aging-Alzheimer's Association workgroups on diagnostic guidelines for Alzheimer's disease. *Alzheimer's & Dementia* 2011; **7**: 263–269.

26 Petersen RC, Smith GE, Waring SC, Ivnik RJ, Tangalos EG, Kokmen E. Mild Cognitive Impairment: Clinical Characterization and Outcome. *Archives of Neurology* 1999; **56**: 303–308.

27 Ottoy J, Ozzoude M, Zukotynski K, Adamo S, Scott C, Gaudet V *et al.* Vascular burden and cognition: Mediating roles of neurodegeneration and amyloid-PET. *Alzheimers Dement* 2022.

28 Duchesne S, Chouinard I, Potvin O, Fonov VS, Khademi A, Bartha R *et al.* The Canadian Dementia Imaging Protocol: Harmonizing National Cohorts. *Journal of Magnetic Resonance Imaging* 2019; **49**: 456–465.

29 Ozzoude M, Ramirez J, Raamana PR, Holmes MF, Walker K, Scott CJM *et al.* Cortical Thickness Estimation in Individuals With Cerebral Small Vessel Disease, Focal Atrophy, and Chronic Stroke Lesions. *Frontiers in Neuroscience* 2020; **14**: 1330.

30 Ramirez J, Gibson E, Quddus A, Lobaugh NJ, Feinstein A, Levine B *et al.* Lesion Explorer: A comprehensive segmentation and parcellation package to obtain regional volumetrics for subcortical hyperintensities and intracranial tissue. *NeuroImage* 2011; **54**: 963–973.

31 Mojiri Forooshani P, Biparva M, Ntiri EE, Ramirez J, Boone L, Holmes MF *et al.* Deep Bayesian networks for uncertainty estimation and adversarial resistance of white matter hyperintensity segmentation. *Human Brain Mapping* 2022; **43**: 2089–2108.

32 Ntiri EE, Holmes MF, Forooshani PM, Ramirez J, Gao F, Ozzoude M *et al.* Improved Segmentation of the Intracranial and Ventricular Volumes in Populations with Cerebrovascular Lesions and Atrophy Using 3D CNNs. *Neuroinform* 2021; **19**: 597–618.

33 Nir TM, Jahanshad N, Villalon-Reina JE, Toga AW, Jack CR, Weiner MW *et al.* Effectiveness of regional DTI measures in distinguishing Alzheimer's disease, MCI, and normal aging. *NeuroImage: Clinical* 2013; **3**: 180–195.

34 Jack CR, Lowe VJ, Senjem ML, Weigand SD, Kemp BJ, Shiung MM *et al.* 11C PiB and structural MRI provide complementary information in imaging of Alzheimer's disease and amnestic mild cognitive impairment. *Brain* 2008; **131**: 665–680.

35 Duering M, Finsterwalder S, Baykara E, Tuladhar AM, Gesierich B, Konieczny MJ *et al.* Free water determines diffusion alterations and clinical status in cerebral small vessel disease. *Alzheimers Dement* 2018; **14**: 764–774.

36 Pasternak O, Westin C-F, Bouix S, Seidman LJ, Goldstein JM, Woo T-UW *et al.* Excessive Extracellular Volume Reveals a Neurodegenerative Pattern in Schizophrenia Onset. *Journal of Neuroscience* 2012; **32**: 17365–17372.

37 Kalheim LF, Bjørnerud A, Fladby T, Vegge K, Selnes P. White matter hyperintensity microstructure in amyloid dysmetabolism. *J Cereb Blood Flow Metab* 2017; **37**: 356–365.

38 Douaud G, Jbabdi S, Behrens TEJ, Menke RA, Gass A, Monsch AU *et al.* DTI measures in crossing-fibre areas: Increased diffusion anisotropy reveals early white matter alteration in MCI and mild Alzheimer's disease. *NeuroImage* 2011; **55**: 880–890.

39 Bergamino M, Walsh RR, Stokes AM. Free-water diffusion tensor imaging improves the accuracy and sensitivity of white matter analysis in Alzheimer's disease. *Sci Rep* 2021; **11**: 6990.

40 Baker SL, Harrison TM, Maass A, La Joie R, Jagust WJ. Effect of Off-Target Binding on ^{18}F-Flortaucipir Variability in Healthy Controls Across the Life Span. *J Nucl Med* 2019; **60**: 1444–1451.

41 Lowe VJ, Lundt ES, Senjem ML, Schwarz CG, Min H-K, Przybelski SA *et al.* White Matter Reference Region in PET Studies of ^{11}C-Pittsburgh Compound B Uptake: Effects of Age and Amyloid-β Deposition. *J Nucl Med* 2018; **59**: 1583–1589.

42 Pietroboni AM, Colombi A, Carandini T, Sacchi L, Fenoglio C, Marotta G *et al.* Amyloid PET imaging and dementias: potential applications in detecting and quantifying early white matter damage. *Alzheimer's Research & Therapy* 2022; **14**: 33.

43 Reginold W, Sam K, Poublanc J, Fisher J, Crawley A, Mikulis DJ. Impact of white matter hyperintensities on surrounding white matter tracts. *Neuroradiology* 2018; **60**: 933–944.

44 Weller RO, Djuanda E, Yow H-Y, Carare RO. Lymphatic drainage of the brain and the pathophysiology of neurological disease. *Acta Neuropathol* 2008; **117**: 1.

45 Charidimou A, Hong YT, Jäger HR, Fox Z, Aigbirhio FI, Fryer TD *et al.* White Matter Perivascular Spaces on Magnetic Resonance Imaging. *Stroke* 2015; **46**: 1707–1709.

46 Iliff JJ, Wang M, Liao Y, Plogg BA, Peng W, Gundersen GA *et al.* A Paravascular Pathway Facilitates CSF Flow Through the Brain Parenchyma and the Clearance of Interstitial Solutes, Including Amyloid β. *Sci Transl Med* 2012; **4**: 147ra111.

47 Maillard P, Fletcher E, Lockhart SN, Roach AE, Reed B, Mungas D *et al.* White Matter Hyperintensities and their Penumbra Lie Along a Continuum of Injury In The Aging Brain. *Stroke* 2014; **45**: 1721–1726.

48 Kalheim LF, Fladby T, Coello C, Bjørnerud A, Selnes P. [18F]-Flutemetamol Uptake in Cortex and White Matter: Comparison with Cerebrospinal Fluid Biomarkers and [18F]-Fludeoxyglucose. *JAD* 2018; **62**: 1595–1607.

49 Pasi M, Salvadori E, Poggesi A, Ciolli L, Del Bene A, Marini S *et al.* White matter microstructural damage in small vessel disease is associated with Montreal cognitive assessment but not with mini mental state examination performances: vascular mild cognitive impairment Tuscany study. *Stroke* 2015; **46**: 262–264.

50 Maillard P, Fletcher E, Singh B, Martinez O, Johnson DK, Olichney JM *et al.* Cerebral white matter free water: A sensitive biomarker of cognition and function. *Neurology* 2019; **92**: e2221–e2231.

51 Makedonov I, Black SE, MacIntosh BJ. Cerebral small vessel disease in aging and Alzheimer's disease: a comparative study using MRI and SPECT. *Eur J Neurol* 2013; **20**: 243–250.

52 Ottoy J, Verhaeghe J, Niemantsverdriet E, Engelborghs S, Stroobants S, Staelens S. A simulation study on the impact of the blood flow-dependent component in [18F]AV45 SUVR in Alzheimer's disease. *PLoS ONE* 2017; **12**: e0189155.

Figures

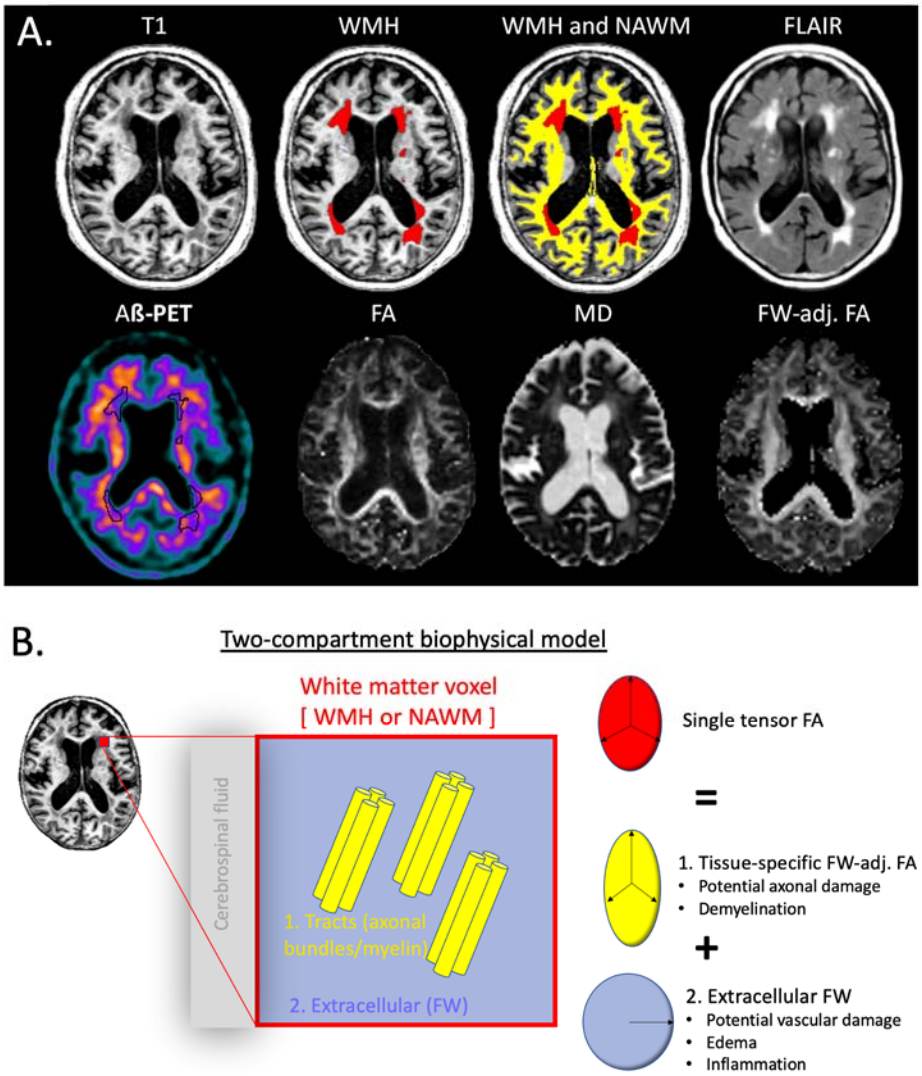

Figure 1. **Methods.** A) Imaging acquisitions and segmentations in a representative subject. (Upper panel, left to right:) T1-weighted scan, T1w image with WMH delineation (red),

T1w image with delineation of both WMH (red) and NAWM (yellow), FLAIR image. (Lower panel, left to right:) ^{18}F-AV45 PET, FA, MD, and FW-adjusted FA maps showing altered signal in the regions of WMH. B) Schematic representation of the two-compartment biophysical DTI model. Each brain voxel (red color) of the NAWM or WMH can be separated into two compartments: an extracellular (FW; purple color) and a fiber-specific (FW-adjusted FA; yellow color) compartment. The 'adjusted' tissue diffusion ellipsoid is more prolate (yellow tensor) after being separated from the isotropic diffusion ellipsoid (purple tensor). Abbreviations: FA, fractional anisotropy; FW, free water; NAWM, normal-appearing white matter; WMH, white matter hyperintensities.

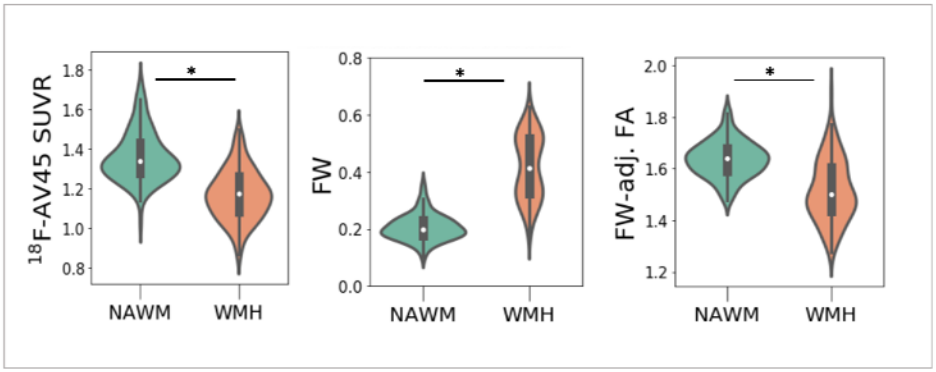

Figure 2. **Differences in ^{18}F-AV45 SUVR and DTI metrics between regions of WMH and NAWM**. Violin plots representing the group differences in SUVR (left panel), FW (middle panel), and FW-adjusted FA (right panel) in the WMH (orange) vs. NAWM (green) across all subjects. Paired t-test showed significant differences between WMH and NAWM at *P<0.0001 for all metrics. Specifically, SUVR and FW-adjusted FA were significantly lower and FW higher in WMH compared to NAWM. Abbreviations: FA, fractional anisotropy; FW, free water; NAWM, normal appearing white matter; SUVR, standardized uptake value ratio; WMH, white matter hyperintensities.

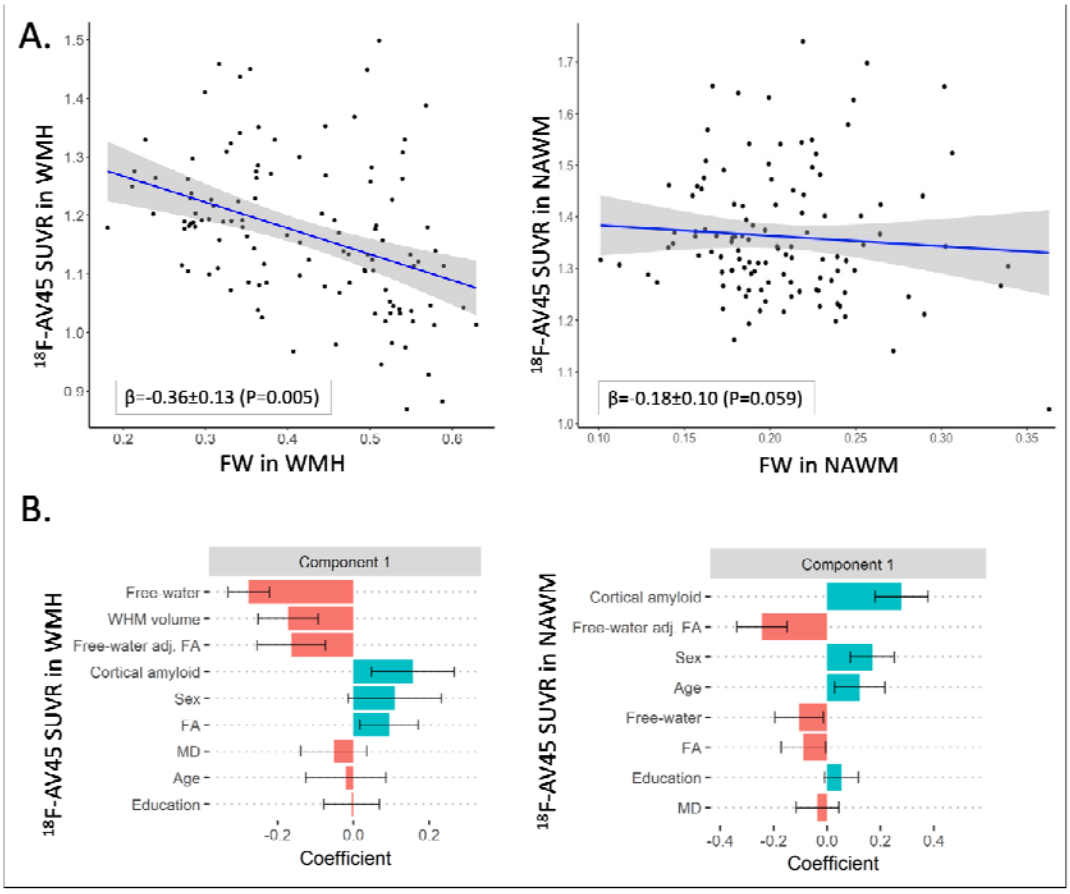

Figure 3. **Relationship between FW and ^{18}F-AV45 SUVR.** A) Increased FW is associated with reduced SUVR in WMH (left) but not in NAWM (right). B) PLS analysis showing how DTI metrics covary together in predicting SUVR in regions of the WM. The plots represent the contribution of the loadings to the first component of PLS analysis

explaining most of the variance in SUVR in WMH (left) and NAWM (right) in the high WMH group. Predictors include DTI metrics (FA, MD, FW, and FW-adjusted FA), demographics (age, sex, education), and imaging variables (WMH volume and cortical Aβ SUVR). Predictors are ordered based on the absolute value of the loading: FW and WMH volume had the most influence on signal in the WMH while cortical Aβ and FW-adjusted FA had the most influence on signal in the NAWM. Error bars represent 95%CI based on bootstrapping with 5,000 repetitions. Results with all subjects combined are represented in Supplementary Figure 2. Abbreviations: FW, free water; MD, mean diffusivity; NAWM, normal appearing white matter; SUVR, standardized uptake value ratio; WMH, white matter hyperintensities

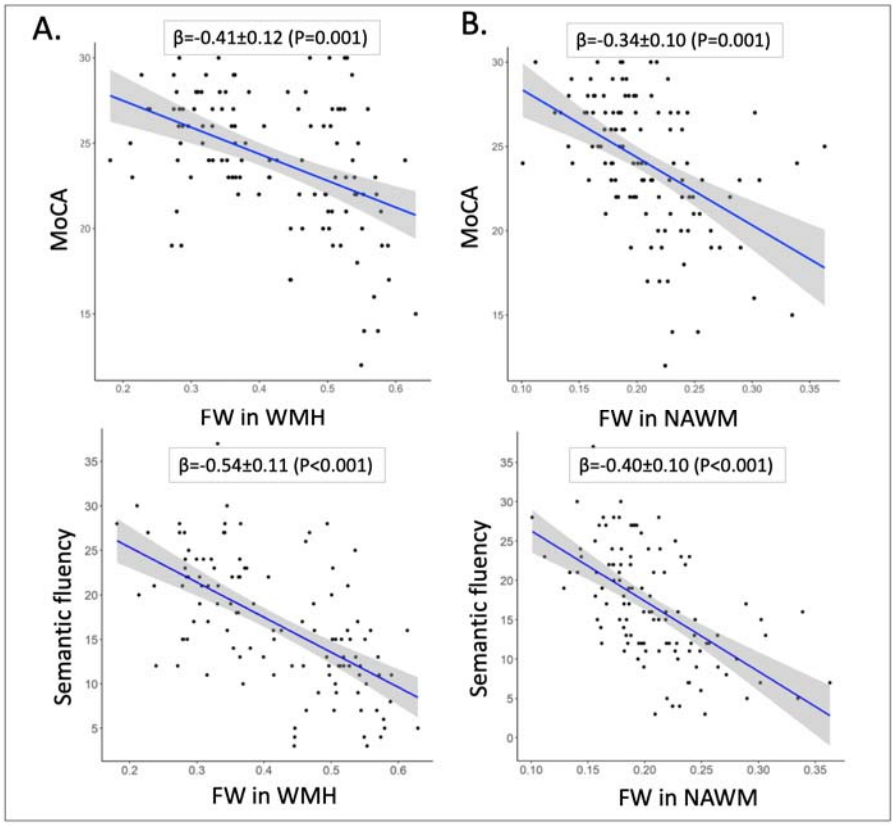

Figure 4. **Associations between FW and cognition.** Increased FW in the WMH (panel A) or NAWM (panel B) associate with cognitive impairment, including MoCA (upper row) and semantic fluency (lower row), across all subjects. Abbreviations: bs, bootstrap; FW, free water; MoCA, Montreal Cognitive Assessment; NAWM, normal appearing white matter; WMH, white matter hyperintensities.

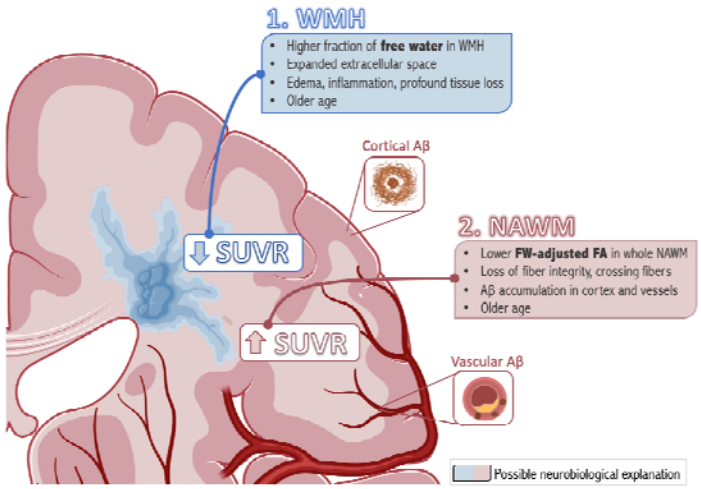

Figure 5. Summary of relationships between ^{18}F-AV45 SUVR and DTI metrics in WM, along with potential neurobiological explanations. Abbreviations: FW-adjusted FA, free water-adjusted fractional anisotropy; NAWM, normal-appearing white matter; SUVR, standardized uptake value ratio derived from amyloid-PET; WMH, white matter hyperintensities [created with BioRender.com]

Tables

Table 1. Demographics. Demographics within the low and high WMH groups. All values are indicated as mean ± standard deviation. Abbreviations: MMSE, Mini-Mental State Examination; MoCA, Montreal Cognitive Assessment; TMT, Trail Making Test; WMH, white matter hyperintensity volumes.

Variables[*]	**Low WMH group (N = 57)**	**High WMH group (N = 58)**	*Test-statistic*
Age (years)	74.14 ± 5.58	76.90 ± 8.13	$t = -2.12^{*}$
Sex female, *N* (%)	34 (60)	26 (45)	$\chi^2 = 1.97$
Education (years)	16.02 ± 2.72	14.29 ± 2.59	$t = 3.48^{**}$
Composite [^{18}F]AV45 SUVR[1]	0.98 ± 0.18	1.12 ± 0.23	$t = -3.59^{***}$
Aβ-positive, *N* (%)	13 (23%)	27 (47%)	$\chi^2 = 7.15^{**}$
Total WMH (cm^3)	10.62 ± 12.93	34.65 ± 18.93	$t = -7.94^{***}$
Body mass index	27.51 ± 5.85	27.32 ± 5.23	t = 0.18
Hypertension[2]**, *N* (%)**	28 (49%)	35 (60%)	$\chi^2 = 1.46$

Smoking, *N* (%)	32 (56%)	23 (40%)	$\chi^2 = 2.85$
Semantic fluency (animals)	20.91 ± 5.70	12.72 ± 6.01	$t = 7.50^{***}$
Boston Naming Test	27.70 ± 2.13	23.65 ± 5.75	$t = 4.78^{***}$
TMT-A (seconds)	36.47 ± 11.36	58.16 ± 33.22	$t = -4.70^{***}$
TMT-B (seconds)	95.79 ± 50.77	187.54 ± 85.74	$t = -6.95^{***}$
MMSE	28.82 ± 1.45	27.10 ± 2.48	$t = 4.53^{***}$
MoCA	25.63 ± 2.53	22.57 ± 4.38	$t = 4.58^{***}$

*P<0.05, **P<0.01, ***P<0.001 using two-tailed t-test (continuous variable) or chi-square (categorical variables).

[1] Referenced to the whole cerebellum.

[2] Hypertension was defined as systolic blood pressure ≥ 140 mmHg and/or diastolic blood pressure ≥ 90 mmHg.

Table 2. Association between DTI metrics and cognition in regions of WMH and NAWM. The regression analyses were adjusted for age, sex, education, WMH volume, and global cortical Aβ SUVR. They were evaluated in both all subjects combined and in the high WMH groups separately. Abbreviations: bs, bootstrap (1,000 repetitions); FA, fractional anisotropy; FW, free water; MMSE, Mini-Mental State Examination; MoCA, Montreal cognitive assessment; WMH, white matter hyperintensities

Regions of white matter hyperintensities						
All subjects (n=115)						
	FW			**FW-adjusted FA**		
	β	*P*	95%CI_{bs}	β	*P*	95%CI_{bs}
Semantic	-0.54	***<0.0001***	-0.78,-0.29	+0.14	***0.084***	-0.03,+0.31
Language	-0.38	***0.002***	-0.65,-0.10	+0.17	***0.050***	+0.03,+0.34
MoCA	-0.41	***0.001***	-0.69,-0.12	+0.17	***0.048***	-0.003,+0.33
MMSE	-0.40	***0.003***	-0.67,-0.10	+0.14	*0.11*	-0.02,+0.32
Speed	+0.31	***0.016***	+0.01,0.58	-0.07	*0.44*	-0.22,+0.08
Executive	+0.35	***0.002***	+0.10,+0.59	-0.10	*0.19*	-0.26,+0.05

High WMH group (n=58)						
	FW			**FW-adjusted FA**		
	β	*P*	95%CI_{bs}	β	*P*	95%CI_{bs}
Semantic	-0.26	***0.059***	-0.54,+0.02	+0.08	*0.58*	-0.16,+0.32
Language	-0.40	***0.003***	-0.68,-0.15	+0.23	***0.091***	-0.05,+0.47
MoCA	-0.34	***0.013***	-0.61,-0.04	+0.11	*0.41*	-0.14,+0.39
MMSE	-0.31	***0.036***	-0.52,-0.03	+0.08	*0.61*	-0.18,+0.41
Speed	+0.08	*0.56*	-0.21,+0.41	-0.11	*0.45*	-0.33,+0.14
Executive	+0.20	*0.15*	-0.01,+0.48	-0.17	*0.20*	-0.52,+0.07

Region of normal-appearing white matter

All subjects (n=115)						
	FW			**FW-adjusted FA**		
	β	*P*	95%CI_{bs}	β	*P*	95%CI_{bs}
Semantic	-0.40	***<0.0001***	-0.61,-0.21	+0.03	*0.71*	-0.14,+0.22
Language	-0.23	***0.032***	-0.42,-0.05	+0.18	***0.034***	-0.03,+0.40

MoCA	-0.34	***0.001***	-0.60,-0.11	+0.10	*0.23*	-0.09,+0.31
MMSE	-0.30	***0.010***	-0.54,-0.09	+0.21	***0.020***	+0.01,+0.41
Speed	+0.32	***0.003***	+0.08,+0.53	+0.05	*0.59*	-0.12,+0.22
Executive	+0.23	***0.021***	+0.04,+0.42	-0.05	*0.49*	-0.21,+0.09
High WMH group (n=58)						
	FW			**FW-adjusted FA**		
	β	*P*	95%CI_{bs}	β	*P*	95%CI_{bs}
Semantic	-0.40	***0.006***	-0.67,-0.09	-0.14	*0.35*	-0.37,+0.16
Language	-0.27	***0.064***	-0.56,+0.03	+0.09	*0.53*	-0.16,+0.43
MoCA	-0.32	***0.028***	-0.65,-0.01	-0.01	*0.93*	-0.29,+0.29
MMSE	-0.36	***0.018***	-0.68,-0.11	+0.08	*0.60*	-0.25,+0.39
Speed	+0.24	*0.10*	-0.07,+0.52	+0.14	*0.33*	-0.10,+0.45
Executive	+0.15	*0.30*	-0.11,+0.42	-0.08	0.59	-0.32,+0.14

Following cognitive tests were applied. Semantic fluency: animal naming; Language: BNT; Speed: TMT-A; Executive function: TMT-B